Proceedings 10th NUMGE 2023
10th European Conference on Numerical Methods in Geotechnical Engineering
Zdravkovic L, Kontoe S, Taborda DMG, Tsiampousi A (eds)

https://doi.org/10.53243/NUMGE2023-149

Finite element analyses of an inhomogeneous bentonite barrier for geological radioactive waste disposal applications

G. Pedone[1] , L. Zdravkovic[2] , D.M. Potts[2] , A. Tsiampousi[2]

[1] *Formerly: Civil and Environmental Engineering Department, Imperial College London, London, UK*
Currently: Civil Environmental and Mechanical Engineering Department, University of Trento, Trento, Italy
[2] *Civil and Environmental Engineering Department, Imperial College London, London, UK*

ABSTRACT: Engineered barriers employed in geological radioactive waste repositories are usually formed of compacted unsaturated bentonite blocks, often used together with bentonite pellets. Compacted bentonite blocks have very low permeabilities, hence their saturation can take hundreds of years. Predicting the bentonite behaviour over such a long time frame is challenging, given that representative laboratory or field experiments over a similar time are unfeasible. In this scenario, numerical tools enable predictive assessments of the long-term barrier performance. The paper reports the results of hydro-mechanically coupled Finite Element (FE) analyses conducted to assess the long-term response of the KBS-3 design scheme developed in Sweden by SKB. Two 2D axisymmetric FE analyses were conducted, simulating two different barrier saturation scenarios, i.e. fast and slow hydration. The simulations were conducted with the code ICFEP, using a constitutive model capable of reproducing the hydro-mechanical behaviour of unsaturated expansive soils with a dual-porosity structure. The analyses verified the long-term safety requirements of the inhomogeneous block-and-pellet bentonite barrier adopted in the KBS-3 scheme.

Keywords: radioactive waste disposal; bentonite barrier; unsaturated expansive soil; finite element modelling

1 INTRODUCTION

Disposal of high heat generating radioactive waste in deep geological formations generally includes bentonite barriers, the latter installed to shield the surrounding host rock from the canister containing the waste. The evolution of the hydro-mechanical properties of bentonite barriers over time has to be carefully assessed by designers, in order to satisfy the repository safety criteria in the long-term (i.e. several hundreds of years after installation).

When installed, bentonite barriers are unsaturated and, therefore, the evolution of their mechanical properties over time depends on the transient seepage processes regulating water flow from the surrounding host rock to the bentonite. Engineered barriers are usually formed of compacted bentonite blocks, often employed in combination with bentonite pellets, the latter used to fill the gaps between blocks and the host rock interface.

Compacted bentonite blocks are characterised by very low hydraulic conductivity, hence their saturation can take from several decades to several hundreds of years. Predicting the bentonite behaviour over such long time frames represents a significant challenge for design engineers, given that fully representative laboratory or field experiments are unfeasible. In this scenario, numerical tools, such as Finite Element (FE) codes, enable predictive assessments of the barrier performance in the long term.

The present work reports some of the results of isothermal hydro-mechanically coupled FE analyses, conducted at Imperial College London as part of the European project BEACON (Bentonite Mechanical Evolution) to assess the long term performance of an inhomogeneous bentonite barrier employed in a radioactive waste repository. The numerical simulations reproduce the KBS-3 design scheme developed in Sweden by SKB, that envisages the combined use of MX-80 bentonite high-density blocks and pellets for backfilling of tunnel construction gaps (Sellin et al., 2017).

Two-dimensional (2D) axisymmetric FE analyses were conducted, accounting for the variability of the tunnel cross-sectional area (i.e. the thickness variability of the pelletised bentonite layer). Two bentonite hydration scenarios were considered, related to two hydraulic boundary conditions imposed by the host rock on the barrier: (i) application, at the rock/bentonite interface, of pore water pressures representative of repository depth; and (ii) a low water inflow allowing for full saturation to take place over ≈4000 years (aimed at reproducing the scenarios of free and restricted access to water, respectively).

The simulations were conducted with the Imperial College Finite Element Programme (ICFEP) (Potts and Zdravković, 1999; 2001), employing the Imperial College dual-porosity structure model (IC-DSM), an advanced constitutive model capable of simulating the

hydro-mechanical behaviour of unsaturated expansive soils (Ghiadistri, 2019; Ghiadistri et al., 2018). The IC-DSM model was used in combination with a variable hydraulic conductivity (HC) model (Nyambayo and Potts, 2010; Potts and Zdravković, 1999) and a void ratio-dependant soil water retention (SWR) model (Melgarejo Corredor, 2004; van Genuchten, 1980).

The paper first presents a brief description of the hydro-mechanical models used in the analyses, followed by a discussion regarding their calibration. The geometry of the boundary value problem analysed and its discretisation are subsequently presented, together with the initial and boundary conditions employed. The main results of the numerical simulations are discussed at the end of the paper, together with key conclusions.

2 HYDRO-MECHANICAL MODELS

2.1 Description of the mechanical model

The Imperial College dual-porosity structure model (IC-DSM) (Ghiadistri, 2019; Ghiadistri et al., 2018) is an extension of the IC single structure model (IC-SSM) (Georgiadis et al., 2005; Tsiampousi et al., 2013), the latter developed based on the Barcelona Basic Modelling (BBM) framework introduced by Alonso et al. (1990). The model adopts two independent stress variables: (i) suction, $s = u_{air} - u_w$, and (ii) net stress, $\bar{\sigma} = \sigma_{tot} - u_{air}$ (u_{air} is the air pressure, u_w is the water pressure, σ_{tot} is the total stress).

The smooth transition between saturated and unsaturated conditions is guaranteed by introducing: (i) an equivalent suction, $s_{eq} = s - s_{air}$, and (ii) an equivalent stress, $\sigma = \bar{\sigma} + s_{air}$ (s_{air} is the air-entry value). The model is further generalised in the (J, p, θ, s_{eq}) space (J is the generalised deviatoric stress, p is the mean equivalent stress, θ is the Lode's angle).

To allow for the modelling of unsaturated expansive clays, a double-porosity structure has been accounted for in the model, following Alonso et al. (1999) and Gens and Alonso (1992). The two levels of structure correspond to: (i) a macro-structure, whose mechanical behaviour is ruled by the BBM-based IC-SSM formulation; (ii) a micro-structure, assumed to be elastic, volumetric and fully saturated.

2.1.1 Double-porosity structure formulation

Given that the micro-structure is assumed to be elastic, volumetric and fully saturated, its deformations are fully defined as:

$$\Delta\varepsilon_{v,m}^{e} = \Delta p' / K_m \tag{1}$$

where the mean effective stress, p', and the micro-structural bulk modulus, K_m, are defined as:

$$p' = p + s_{eq} \tag{2}$$

$$K_m = [(1 + e_m)/\kappa_m] \cdot p' \tag{3}$$

In Equation (3), e_m is the micro-structural void ratio and κ_m is the micro-structural elastic compressibility parameter. The overall void ratio, e, is obtained by adding e_m and e_M, where the latter represents the macro-structural void ratio. The model also introduces a void factor, $VF = e_m/e$, that is automatically set to zero when fully saturated conditions are attained. The bulk modulus, K_m, is additional to the two bulk moduli, $K_{s,M}$ and $K_{p,M}$, associated with the macro-structure and related to equivalent suction and mean equivalent stress variations, respectively.

Although the micro-structural volumetric deformations are elastic, they are assumed to contribute to the macro-structural volumetric plastic strains, $\Delta\varepsilon_{v,\beta}^{p}$, through an additional plastic mechanism:

$$\Delta\varepsilon_{v,\beta}^{p} = f_\beta \cdot \Delta\varepsilon_{v,m}^{e} \tag{4}$$

defined by the interaction function, f_β, between the two levels of structure. The shape of this function is dependent on whether the micro-structure swells (S) or compresses (C) and is defined as:

$$f_\beta \begin{cases} C \begin{cases} c_{c1} + c_{c2}(p_r/p_0)^{c_{c3}} & (p_r/p_0 \geq 0) \\ c_{c1} & (p_r/p_0 < 0) \end{cases} \\ S \begin{cases} c_{s1} + c_{s2}(1 - p_r/p_0)^{c_{s3}} & (p_r/p_0 \geq 0) \\ c_{s1} + c_{s2} & (p_r/p_0 < 0) \end{cases} \end{cases} \tag{5}$$

where p_r and p_0 represent the current stress state and the hardening parameter defining the size of the yield surface, respectively, while c_{c1}, c_{c2}, c_{c3} and c_{s1}, c_{s2}, c_{s3} are coefficients defining the shape of the interaction function.

2.2 Description of the hydraulic models

A non-hysteretic van Genuchten-type (1980) SWR model was adopted, formulated in terms of degree of saturation, S_r, and equivalent suction, s_{eq} (Melgarejo Corredor, 2004):

$$S_r = \left\{ \frac{1}{1 + [\alpha \cdot (\nu - 1)^{\psi} \cdot s_{eq}]^n} \right\}^m \cdot (1 - S_{r0}) + S_{r0} \tag{6}$$

where: S_{r0} is the residual degree of saturation; α, m and n are fitting parameters controlling the shape of the water retention curve; ψ is the parameter controlling the effect of the specific volume, ν.

The HC model used in the numerical simulations (Nyambayo and Potts, 2010; Potts and Zdravković, 1999) assumes the hydraulic conductivity, k, to vary with suction according to the following equation:

$$\log k = \log k_{sat} - \frac{(s-s_1)}{(s_2-s_1)} \cdot \log \frac{k_{sat}}{k_{min}} \qquad (7)$$

where k_{sat} is the saturated hydraulic conductivity (for $s < s_1$), k_{min} is the minimum k (for $s > s_2$).

2.3 Selection of the model parameters

The model parameters used in the analyses are reported in Tables 1, 2 and 3, with reference to the IC-DSM model, the SWR model, and the HC model, respectively. For the MX-80 bentonite blocks, the parameters were derived from laboratory data reported in Bosch et al. (2019), Dueck and Nilsson (2010), Marcial et al. (2008), Seiphoori et al. (2014), Tang and Cui (2010). For the MX-80 bentonite pellets, the parameters were derived from laboratory data reported in Alonso et al. (2011), Hoffman et al. (2007), Toprak et al. (2020).

Table 1. Input parameters for IC-DSM model

Parameter	Blocks	Pellets
Yield surface, $\boldsymbol{M_F, \alpha_F, \mu_F}$	0.495,0.4,0.9	1.00,0.4,0.9
Plastic potential, $\boldsymbol{\alpha_G, \mu_G}$	0.4,0.9	0.4,0.9
Critical state ratio, $\boldsymbol{M_J}$	0.495	1.00
Charact. pressure, $\boldsymbol{p_c}$(kPa)	1000.0	50.0
Specific volume at unit pressure, $\boldsymbol{v_1(s_{eq})}$	5.847	4.020
Saturated plastic compressibility, $\boldsymbol{\lambda(0)}$	0.515	0.226
Elastic compressibility, $\boldsymbol{\kappa}$	0.0087	0.045
Maximum soil stiffness, $\boldsymbol{r}$	0.800	0.800
Soil stiffness increase, $\boldsymbol{\beta}$(1/kPa)	8.5×10^{-5}	10^{-7}
Elastic compressibility (for $\boldsymbol{\Delta s_{eq}}$), $\boldsymbol{\kappa_s}$	0.142	0.010
Poisson's ratio, $\boldsymbol{\mu}$	0.3	0.2
Plastic compressibility (for $\boldsymbol{\Delta s_{eq}}$), $\boldsymbol{\lambda_s}$	0.566	0.040
Air-entry value, $\boldsymbol{s_{air}}$(kPa)	1000.0	0.0
$\boldsymbol{s_{eq}}$ yield value, $\boldsymbol{s_0}$(kPa)	10^6	10^6
Micro-structural compressibility, $\boldsymbol{\kappa_m}$	0.360	0.090
Void factor, **VF**	0.457	0.163
$\mathbf{f_\beta}$ micro-swelling/ micro-compression, $\mathbf{c_{s1}, c_{s2}, c_{s3}/c_{c1}, c_{c2}, c_{c3}}$	-0.2,1.2,3.0	-0.1,1.1,3.0

The predictive capabilities of the mechanical model, when adopting the parameters in Tables 1, 2 and 3 to simulate the behaviour of MX-80 blocks, can be evaluated from Figure 1. The figure shows the results of a swelling pressure test for a dry density, ρ_d, and an initial gravimetric water content, w, of 1.7 g/cm^3 and 17%, respectively (compared with expected swelling pressures as reported by Olsson et al. (2013)).

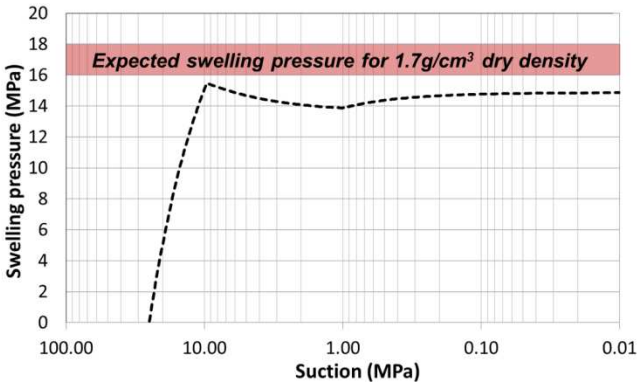

Figure 1. Swelling pressure test results for MX-80 blocks (expected swelling pressure from Olsson et al. (2013))

The SWR model parameters used in the analyses are summarised in Table 2. As an example, Figure 2 shows the SWR curves employed for the MX-80 blocks in comparison with laboratory data from Seiphoori et al. (2014).

Table 2. Input parameters for SWR model

Parameter	Blocks	Pellets
Fitting parameter, $\boldsymbol{\alpha}$(1/kPa)	0.0001	0.0015
Fitting parameter, $\boldsymbol{m}$	0.47	0.25
Fitting parameter, $\boldsymbol{n}$	1.90	1.05
Fitting parameter, $\boldsymbol{\psi}$	2.0	2.5
Residual degree of saturation,$\boldsymbol{S_{r0}}$	0.05	0.0

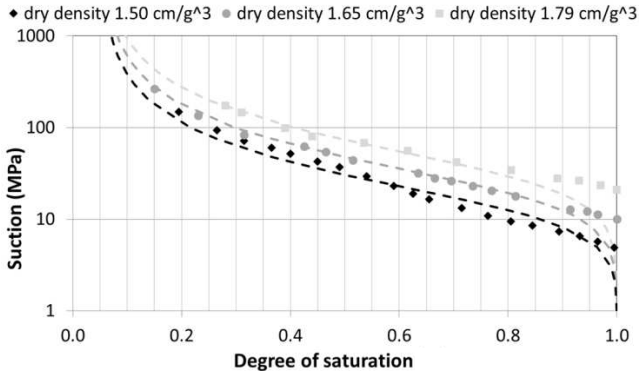

Figure 2. Comparison between adopted SWR curves (dashed lines) and experimental data (symbols) for bentonite blocks (laboratory data from Seiphoori et al. (2014))

The HC model parameters used for the MX-80 bentonite blocks (Table 3) were defined based on the data reported by Marcial et al. (2008), and were adopted in conjunction with a saturated hydraulic conductivity of 3×10^{-14} m/s (Olsson et al., 2013).

Table 3. Input parameters for HC model

Parameter	Blocks	Pellets
Sat. hydr. conductivity, $\boldsymbol{k_{sat}}$(m/s)	3×10^{-14}	5×10^{-10}
Min. hydr. conductivity, $\boldsymbol{k_{min}}$(m/s)	3×10^{-15}	5×10^{-10}
Suction, $\boldsymbol{s_1}$(kPa)	1000.0	N/A
Suction, $\boldsymbol{s_2}$(kPa)	41000.0	N/A

Regarding the pellets, due to their peculiar structure, Hoffman et al. (2007) show that the hydraulic conductivity tends to decrease with suction reductions, contrary to what is more generally observed in geo-materials. The HC model available cannot reproduce such a variation, and, therefore, a constant hydraulic conductivity of 5×10^{-10} m/s was selected for the pellets (Table 3), corresponding to the average value of measurements carried out by Hoffman et al. (2007).

3 KBS-3 SCHEME ANALYSIS

3.1 Geometry and discretisation

All the numerical simulations undertaken were hydro-mechanically fully coupled and were carried out with the FE code ICFEP (Potts & Zdravković, 1999; 2001). Given that the 2 scenarios investigated refer to (global) constant volume conditions, no significant displacements were expected, and, therefore, the small displacement formulation was adopted.

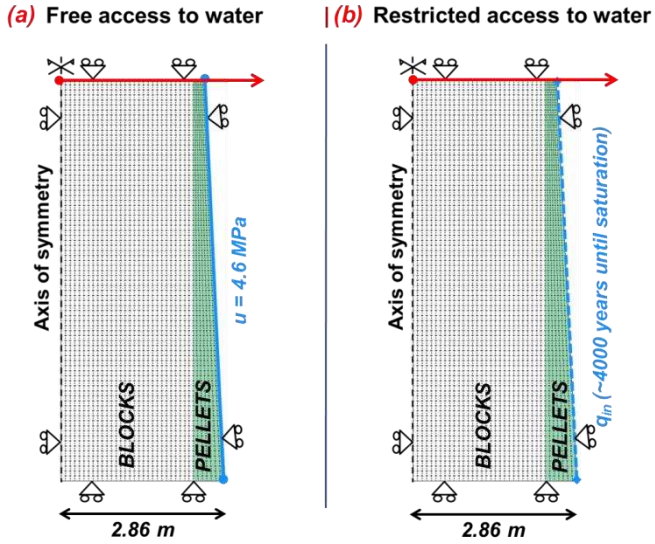

Figure 3. FE mesh and boundary conditions adopted

Due to the axisymmetric nature of the 2 scenarios under investigation (i.e. free access to water and restricted access to water), 2D axisymmetric FE simulations were undertaken. The domain analysed (maximum radius of 2.86 m, length of 7 m) was discretised using 8-noded quadrilateral displacement-based elements, with 4 pore pressure degrees of freedom at the corner nodes. The mesh generated is shown in Figure 3, together with the mechanical and hydraulic boundary conditions adopted for the 2 simulated scenarios.

3.2 Initial and boundary conditions

The initial conditions assumed in the analyses, summarised in Table 4, correspond to those suggested by Leupin et al. (2020). The initial state of the materials is reported by Leupin et al. (2020) in terms of dry densities and gravimetric water contents, so the initial suctions were directly derived from the water retention curves adopted (e.g. Figure 2). An initial nominal isotropic total stress of 100 kPa was assigned to both materials in both analyses.

Table 4. Initial conditions assumed in the FE analyses

Parameter	Blocks	Pellets
Mean total stress, $\boldsymbol{p}$(MPa)	0.1	0.1
Water content, $\boldsymbol{w}$(%)	17.0	17.0
Dry density, $\boldsymbol{\rho_d}$(g/cm^3)	1.7	1.0
Void ratio, $\boldsymbol{e}$(-)	0.635	1.780
Degree of saturation, $\boldsymbol{S_r}$(%)	74.56	26.55
Suction (MPa)	24.995	24.536

The free access to water scenario was modelled by imposing a positive pore pressure of 4.6 MPa on the mesh boundary representing the contact area between MX-80 pellets and the host rock (Figure 3(a)). The 4.6 MPa pore pressure, representative of typical repository depths, was applied gradually, over ≈1.5 years, to avoid large hydraulic gradients. The boundary corresponding to the axis of symmetry, as well as the top and bottom boundaries (Figure 3(a)), were assumed impervious during the entire simulation. The analysis was considered completed when a 4.6 MPa positive pore pressure was observed throughout the whole domain analysed.

The restricted access to water scenario was modelled by applying, in the first part of the analysis, a constant in-flow of 2.1×10^{-12} m/s on the mesh boundary representing the contact area between MX-80 pellets and the host rock (Figure 3(b)). The in-flow magnitude was selected to reach full saturation after ≈4000 years, the latter identified by Sellin et al. (2017) as a representative saturation period in case of restricted access to water. At the end of the saturation period, the hydraulic boundary condition on the right boundary was changed, applying a constant positive pore pressure of 4.6 MPa. Also for the second scenario analysed, top, bottom and left boundaries were assumed impervious, and the analysis was stopped when a 4.6 MPa positive pore pressure was observed everywhere in the mesh.

The mechanical boundary conditions applied in both analyses, i.e. no displacements in the directions orthogonal to the boundaries, are shown in Figure 3.

4 RESULTS

4.1 Free access to water scenario

The analysis suggests that, after ≈1.5 years, the pore pressure in the bentonite pellets corresponds to the one applied at the hydration boundary (i.e. 4.6 MPa), due to the relatively large permeability characterising the pelletised material (Table 3). On the other hand, it takes several decades for the hydration front to pene-

trate the blocks and reach the axis of symmetry, due to the very low permeability characterising the blocks (Table 3). Consequently, even when free access to water is allowed for, the full pore pressure equilibration of the whole barrier is only reached after ≈150 years.

After 1.5 years, when the pore water pressure at the right boundary of the mesh is increased up to 4.6 MPa, a significant increase in mean total stress is already observed across the whole domain analysed (≈8 MPa peak value). After some decades, the hydration front tends to move towards the axis of symmetry of the mesh, causing a further increase in swelling pressure (≈12 MPa maximum values after ≈50 years). The maximum swelling pressure (≈14 MPa) is predicted at the end of the analysis, i.e. after ≈150 years, when a positive pore pressure of 4.6 MPa is reached everywhere in the mesh. The swelling pressure distribution predicted in the long-term at the top boundary of the mesh (red arrow in Figure 3) is shown in Figure 4.

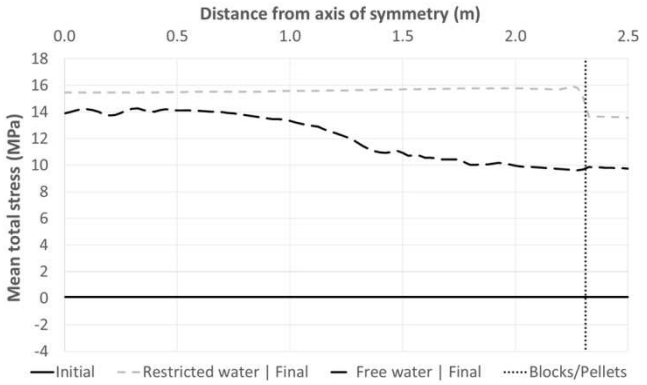

Figure 4. Swelling pressure distributions predicted in the long-term at the top boundary (red arrow in Figure 3)

The gradual increase in swelling pressure induced by the hydration process is associated with a homogenisation of the backfill, as shown in Figure 5, where the final void ratio distribution predicted at the top boundary of the mesh (red arrow in Figure 3) is illustrated.

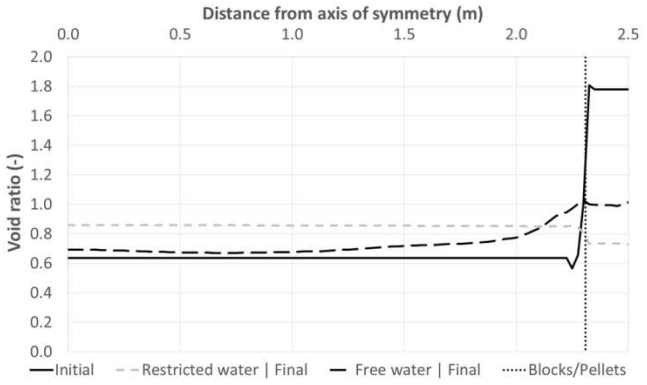

Figure 5. Void ratio distributions predicted in the long-term at the top boundary (red arrow in Figure 3)

The homogenisation process results in significant void ratio reductions for the pellets (from e=1.78 to e≈1.00 at the top boundary of the mesh; Figure 5). The blocks, on the other hand, tend to swell during the hydration process, experiencing less pronounced void ratio variations compared to the pellets. In particular, the long-term void ratio variations appear to be very limited in the proximity of the axis of symmetry (Figure 5), probably because hydration takes place from the outer edge of the domain analysed, so the central area tends to swell almost under fully confined conditions.

4.2 Restricted access to water scenario

In this case, as expected, the pore water pressure increase is significantly slower, as well as more homogeneous throughout the domain. This is a consequence of the inflow rate applied as the boundary condition (i.e. 2.1×10^{-12} m/s), which was selected in order to achieve full saturation after ≈4000 years. After reaching full saturation everywhere in the mesh, the hydraulic boundary condition was changed, and a positive pore pressure of 4.6 MPa was applied instead. Given that the backfill was already fully saturated when the hydraulic boundary condition was changed, the pore pressure increased everywhere towards the value of 4.6 MPa in less than 200 years.

The mean total stress increase is very limited in the first 100 years, with the highest values (<2 MPa) achieved within the blocks located next to the pellets (i.e. closer to the hydration boundary). More significant swelling pressure variations were predicted after around 1000 years (>2 MPa in the pellets and ≈5 MPa in the blocks). As expected, the highest mean total stress values are predicted at the end of the analysis, when values of 16 MPa are approached in the blocks. This is shown in Figure 4, where the swelling pressure distribution predicted in the long-term at the top boundary of the mesh is plotted.

The increase in mean total stress with time is associated with a significant void ratio reduction in the pellets and a comparatively more limited void ratio increase in the blocks (see Figure 5, showing the void ratio distribution predicted in the long-term at the top boundary of the mesh).

It is interesting to observe that a much more homogenous void ratio distribution is achieved at the end of the restricted access to water analysis compared to the free access to water analysis (see Figure 5). This seems to suggest that a slower hydration process leads to a more homogeneous void ratio distribution in the whole bentonite buffer. It is also interesting to observe that the presence of higher swelling pressures in the restricted access to water analysis is associated with more significant void ratio reductions in the pellets, where void ratios even lower than those characterising the blocks are predicted at the end of the analysis.

5 CONCLUSIONS

The following key conclusions can be drawn:

- Even when access to water is not restricted and the pore water pressure acting on the outer surface of the backfill corresponds to values representative of typical repository depths (i.e. 4.6 MPa), the full pore pressure equalisation is achieved after ≈1.5 centuries.
- The maximum mean total stress predicted in the free access to water scenario (representative of the swelling pressures developing within the bentonite buffer) is around 14 MPa. In the restricted access to water scenario, instead, the maximum mean total stress predicted is close to 16 MPa. In both cases, the mean total stresses are exceeding 10 MPa, the latter considered as a limit pressure for the barrier (Leupin et al., 2020).
- During the hydration process, the pellets tend to compress and the blocks tend to swell, resulting in a more homogeneous void ratio distribution after hydration. The numerical simulations suggest that a more pronounced homogenisation is likely to be achieved when slower hydration takes place (e.g. restricted access to water analysis).

6 ACKNOWLEDGEMENTS

The work presented in this paper was part of the European project BEACON (Bentonite Mechanical Evolution), which received funding from the Euratom research and training programme 2014–2018 under grant agreement No 745942.

7 REFERENCES

Alonso, E.E., Gens, A., Josa, A. 1990. A constitutive model for partially saturated soils, *Géotechnique* **40**, 3, 405-430.

Alonso, E.E., Romero, E., Hoffman, C. 2011. Hydromechanical behaviour of compacted granular expansive mixtures: experimental and constitutive study, *Géotechnique* **6**, 4, 329-344.

Alonso, E.E., Vaunat, J., Gens, A. 1999. Modelling the mechanical behaviour of expansive clays, *Engineering Geology* **54**, 1, 173-183

Bosch, J.A., Baryla, P., Ferrari, A. 2019. *BEACON project - Modelling specifications for Task 3.3: Performance of constitutive models developed in the project*, BEACON project, Technical report.

Dueck, A., Nilsson, U. 2010. *Thermo-Hydro-Mechanical properties of MX-80 - Results from advanced laboratory tests*. Technical Report TR-10-55, SKW, Sweden.

Gens, A., Alonso, E.E. 1992. A framework for the behaviour of unsaturated expansive clays, *Canadian Geotechnical Journal* **29**, 6, 1013-1032.

Georgiadis, K., Potts, D.M., Zdravković, L. 2005. Three-dimensional constitutive model for partially and fully saturated soils, *International Journal Geomechanics* **5**, 3, 244-255.

Ghiadistri, G.M. 2019. *Constitutive modelling of compacted clays for applications in nuclear waste disposal*, PhD Thesis, Imperial College London, UK.

Ghiadistri, G.M., Potts, D.M., Zdravković, L., Tsiampousi, A. 2018. A new double structure model for expansive clays. *Proceedings 7th International Conference on Unsaturated Soils, UNSAT, Hong Kong*.

Hoffman, C., Alonso, E.E., Romero, E. 2007. Hydromechanical behaviour of bentonite pellet mixtures, *Physics and Chemistry of the Earth* **32**, 832-849.

Leupin, O., Talandier, J., Sellin, P., Lanyon, G.W. 2020. *BEACON project - Assessment cases for the evaluation of the degree of heterogeneity*, BEACON project, Technical report.

Marcial, D., Delage, P., Cui, Y.J. 2008. Hydromechanical couplings in confined MX80 bentonite during hydration. *Proceedings 1st European Conference on Unsaturated Soils, E-UNSAT, Durham, UK*.

Melgarejo Corredor, M.L. 2004. *Laboratory and numerical investigations of soil retention curves*, PhD Thesis, Imperial College, University of London, UK.

Nyambayo, V.P., Potts, D.M. 2010. Numerical simulation of evapotranspiration using a root water uptake model, *Computers and Geotechnics* **37**, 175-186.

Olsson, S., Jensen, V., Johannesson, L.E., Hansen, E., Karnland, O., Kumpulainen, S., Kiviranta, L., Svensson, D., Karnbranslehantering, S., Hansen, S., Linden, J., Akademi, A. 2013. *Prototype Repository - Hydro-mechanical, chemical and mineralogical characterization of the buffer and tunnel backfill material from the outer section of the Prototype Repository*, SKB, Technical Report TR-13-21.

Potts, D.M., Zdravković, L. 1999. *Finite element analysis in geotechnical engineering: theory*, Thomas Telford Publishing, London, UK.

Potts, D.M., Zdravković, L. 2001. *Finite element analysis in geotechnical engineering: application*, Thomas Telford Publishing, London, UK.

Seiphoori, A., Ferrari, A., Laloui, L. 2014. Water retention behaviour and microstructural evolutions of MX-80 bentonite during wetting and drying cycles, *Géotechnique* **64**, 9, 721-734.

Sellin, P., Akesson, M., Kristensson, O., Malmberg, D., Borgesson, L., Birgersson, M., Dueck, A., Karnland, O., Hernelind, J. 2017. *Long re-saturation phase of a final repository - Additional supplementary information*, SKB, Technical Report TR-17-15.

Tang, A.M., Cui, Y.J. 2010. Experimental study on hydro-mechanical coupling behaviours of highly compacted expansive clay, *Journal of Rock Mechanics and Geotechnical Engineering* **2**, 1, 39-43.

Toprak, E., Olivella, S., Pintado, X. 2020. Modelling engineered barriers for spent nuclear fuel repository using a double-structure model for pellets, *Environmental Geotechnics* **7**, 1, 72-94.

Tsiampousi, A., Zdravković, L., Potts, D.M. 2013. A new Hvorslev surface for critical state type unsaturated and saturated constitutive models, *Computers and Geotechnics* **48**, 156-166.

van Genuchten, M.T. 1980. A closed-form equation for predicting the hydraulic conductivity of unsaturated soils, *Soil Science Society of America Journal* **44**, 892-898.